Surface & Coatings Technology 237 (2013) 369–378

Contents lists available at ScienceDirect

Surface & Coatings Technology

journal homepage: www.elsevier.com/locate/surfcoat

Deposition of aluminum oxide by evaporative coating at atmospheric pressure (ECAP)

Yui Lun Wu *, Jungmi Hong, David Peterson, Jeffrey Zhou, Tae S. Cho, D.N. Ruzic

Center for Plasma Material Interactions, Department of Nuclear Plasma and Radiological Engineering, University of Illinois at Urbana-Champaign, Urbana, IL 61801, USA

ARTICLE INFO

Available online 18 June 2013

Keywords:
Aluminum oxide
Atmospheric pressure
Plasma
Evaporative coating
Microwave
Plasma jet

ABSTRACT

The Center for Plasma-Material Interaction (CPMI) has developed innovative coating method of evaporative coating at atmospheric pressure (ECAP). This new idea is an atmospheric-pressure-based process. Following the similar concept as the laser-assisted plasma coating at atmospheric pressure (LAPCAP) [1], the material captured by the plasma plume is atomic in nature (the evaporated metal atom) and should therefore end up deposited molecule-by-molecule as in a PVD fashion. By using the thermal energy from the microwave plasma, solid 99.99% + purity aluminum were evaporated and then produce a PVD-like alumina coating on a work piece. The aluminum target was inserted in the center of the microwave torch feeding a melt pool and evaporated into the surrounding plasma plume. A bottle neck was made in the antenna and could reduce the heat loss by 84%, thus allowing higher temperatures to exist in the sample-holder antenna tip. Gas shielding was used to keep the work gas pure. The film was deposited as Al_2O_3 using oxygen from the environment. Deposition rate was around 2 μm/min. Gas flow rate around the antenna tip was about 0.9 m/s, and the temperature of the plasma was about 1400 °C at 1350 W input power from simulations. Alpha and other metastable phases of aluminum oxide were found on the deposited films.

1. Introduction

Aluminum oxide (alumina) is one of the most important ceramic materials due to its many appealing properties. It is electrically insulating, optically transparent, mechanically hard and chemically stable, and these properties make it suitable for many different applications [6,10–12]. Alumina could be found in a number of crystalline phases or polymorphs (α, γ, η, δ, κ, χ, etc.), the α phase is thermodynamically stable at any temperatures up to its melting temperature at 2051 °C, but the other metastable phases like γ or θ also appears frequently in alumina growth studies as well [2]. This polymorphism also creates opportunities for applications in various areas of technical science since the properties of one alumina phase may differ from the properties of another [3].

All alumina phases (except the α phase) has a transformation sequences, and the common characteristic in which all they have in common are that they all transform to the α phase at high temperature since the α phase is the only thermodynamically stable phase of alumina. It has the highest density, elastic modulus, hardness and band gap among all phases of alumina, and these properties make it the material of choice for many applications industrially such as chemical and wear protection [2,3,6,10–12]. Fig. 1 illustrates some phase transition relations for the common metastable alumina phases [4,5]. The transformations to the phase from other metastable phases typically take place at above 1000 °C and are all irreversible [3,6].

Currently, the most common method for depositing aluminum oxide is though chemical vapor deposition (CVD). It can be classified mainly as low pressure chemical vapor deposition (LPCVD) or atmospheric pressure chemical vapor deposition (APCVD). In LPCVD, precursor gases are introduced into the vacuum system, and the molecules of the precursor gases will be adsorbed onto the substrate surface. They then will react and the reaction will create solid product, which is the desired film coating, and other product gases. The produced gases will desorb from the substrate surface and be removed by scrubbers and pumps. In the case of aluminum oxide, it can be done by using trimethylaluminum (TMA), aluminum chloride as the precursor in plasma enhanced CVD (PECVD) and aluminum tri-isopropoxide (ATI) with thermal CVD [7]. They can achieve a precise chemical composition, high film quality and uniformity. However, growth rate is comparatively low in CVD systems, usually on the order of 1–10 nm/min [8,9], since only a small fraction of the incoming precursor are going to participate in the film formation, a large portion of the gas entering the chamber would just simply pass through the chamber and removed by the pumps [13]. Also, chlorine and hydrocarbon contaminants are commonly found in the deposited film, and high temperature corrosive gas will be commonly formed as product as well. These products may further react with the alumina film surface before being removed from the chamber and degrade the quality of the film [13].

* Corresponding author. Tel.: +1 2173336291.
E-mail address: wu139@illinois.edu (Y.L. Wu).

0257-8972/$ – see front matter © 2013 Elsevier B.V. All rights reserved.
http://dx.doi.org/10.1016/j.surfcoat.2013.06.043

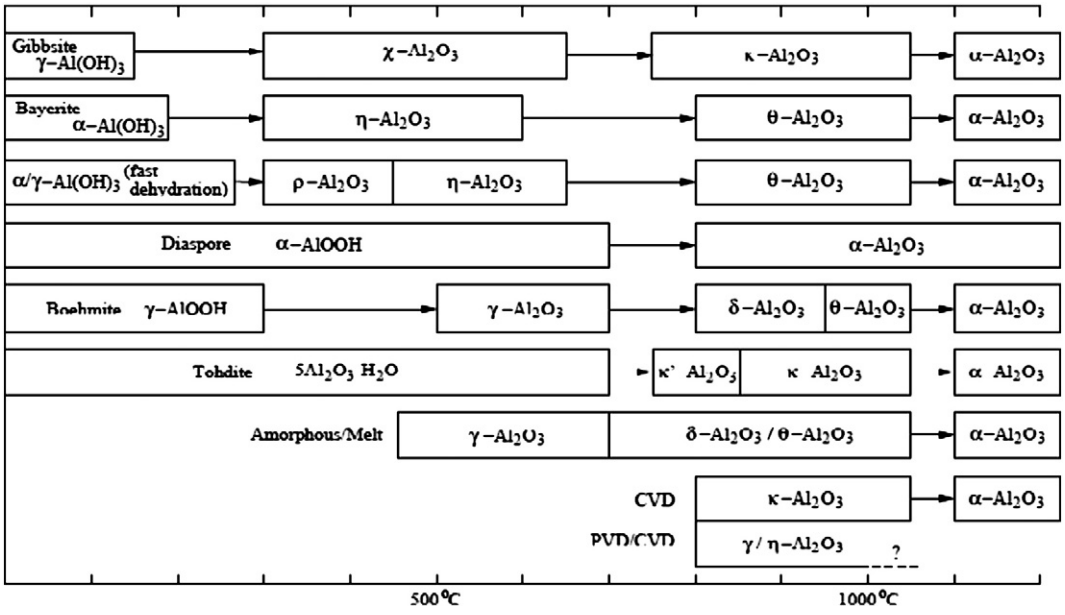

Fig. 1. Commonly accepted transition sequences of the alumina from the hydroxides to corundum (α-Al_2O_3) during thermal treatment [4,5].

For the first time, aluminum oxide thin films will be created by microwave plasma jet under atmospheric pressure conditions. The basic principle behind this technique is to use the heat from the atmospheric plasma to melt and evaporate aluminum metal targets at the tip of the antenna. The vaporized aluminum atom will then be carried by the mixed helium and nitrogen gas flow in the plasma towards the substrate surface. The aluminum adhered to the surface of the stainless substrate surface will then be oxidized by the ambient oxygen in the atmosphere and forming aluminum oxide or alumina coatings.

The benefits of this concept are that no additional heat source other than the plasma will be needed and the phase of the alumina deposited could be modified as plasma condition changes. Compared with other common low pressure process such as RF sputtering or DC reactive sputtering, the ECAP concept can achieve deposition rate of one to two orders of magnitude higher while achieving similar film morphologies and properties [21,22]. Also since it is an atmospheric process, no expensive vacuum chamber or vacuum equipment are needed. Unlike other plasma torch spray processes, the ECAP system does not require an external source of aluminum oxide powder to be brought into the plasma spray to coat the substrate; rather, it uses the aluminum from its antenna and converts it into the aluminum oxide film desired with the microwave power and surrounding oxygen while it reaches the substrate surface. Additionally, it can be easily modified to deposit with different materials or on non-planar surfaces by simply using a gas shield around the torch or implementing automation between the atmospheric torch and the substrate.

2. Experimental

The evaporative coating at atmospheric pressure (ECAP) experiment was powered by a 2.45-GHz microwave source. The microwave is generated by a magnetron in the generator made by Cober Electronics, Inc (Model S6F). It uses a 12-kW power input, and the output varies from approximately 0.5 to 6 kW into a matched load with continuously adjustable power. The waveguide used to transmit microwave power from the magnetron to the atmospheric torch is the WR 284 waveguide cavities. The aluminum E-Band, H-Bend, two-port circulator, dual directional coupler and 4-stub tuning system are all made by CoberMuegge LLC, USA, while the 3-stub tuning system and the WR284 to 7/16 adapter are custom made in the University of Illinois Urbana-Champaign.

The atmospheric pressure plasma torch (APPT) used for the ECAP experiment was designed and fabricated at the University of Illinois Urbana Champaign. It is a three coaxial cylinder design with decreasing diameter closer to the top of the torch. The cylinders were made with copper. The antenna was made with tungsten and connected to the coaxial adapter by a receptacle jack made by HUBER & SUHNER Group, USA and a 7/16 (11 mm) DIN adapter by RF Parts Company, USA. The diameter of the tungsten antenna was ¼" (6.35 mm) in diameter and 6 ¼" (158.75 mm) in length. The quartz discharge tube had an outer diameter of 16.2 mm and an inner diameter of 13 mm, made by the Technical Glass Products, Inc., USA. It was fixed in the inside of the torch by two Teflon rings between the discharge tube and the copper cylinders. The inlet gas is fed into the APPT from the bottom of the outermost copper cylinder, and a Teflon pad was placed at the bottom of the outermost cylinder wall in order to prevent arcing between the antenna and the copper cylinder as well.

All the processing gases (helium, argon, nitrogen, oxygen, hydrogen, etc.) are controlled through various RMA-Master flow meters made by Dwyze Instruments, Inc., USA. They can be individually controlled in order to generate different types of plasma with different gas mixtures.

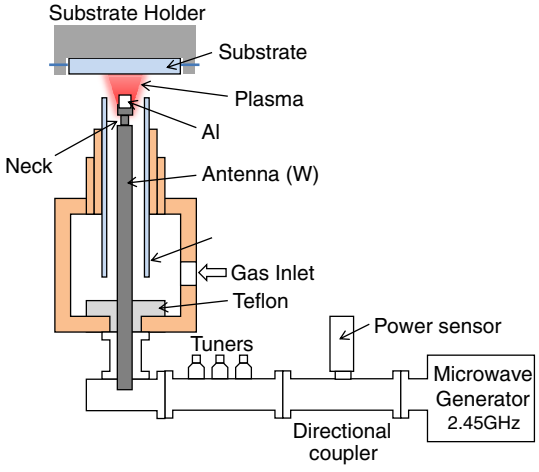

Fig. 2. Schematic figure of the atmospheric pressure plasma torch (APPT) [8].

Fig. 3. Stainless substrate mounted on the substrate holder before (left) and after (right) deposition for the APPT in EVAP experiments.

In the ECAP study, helium and nitrogen are mainly used to create the plasma profile and gas temperature required for the alumina deposition. A schematic figure of the APPT is shown in Fig. 2 [8].

The APPT used in the ECAP study could generate atmospheric pressure plasma (APP) with a plasma gas temperature raging from room temperature to a maximum of 3000 °C, depending on the applied

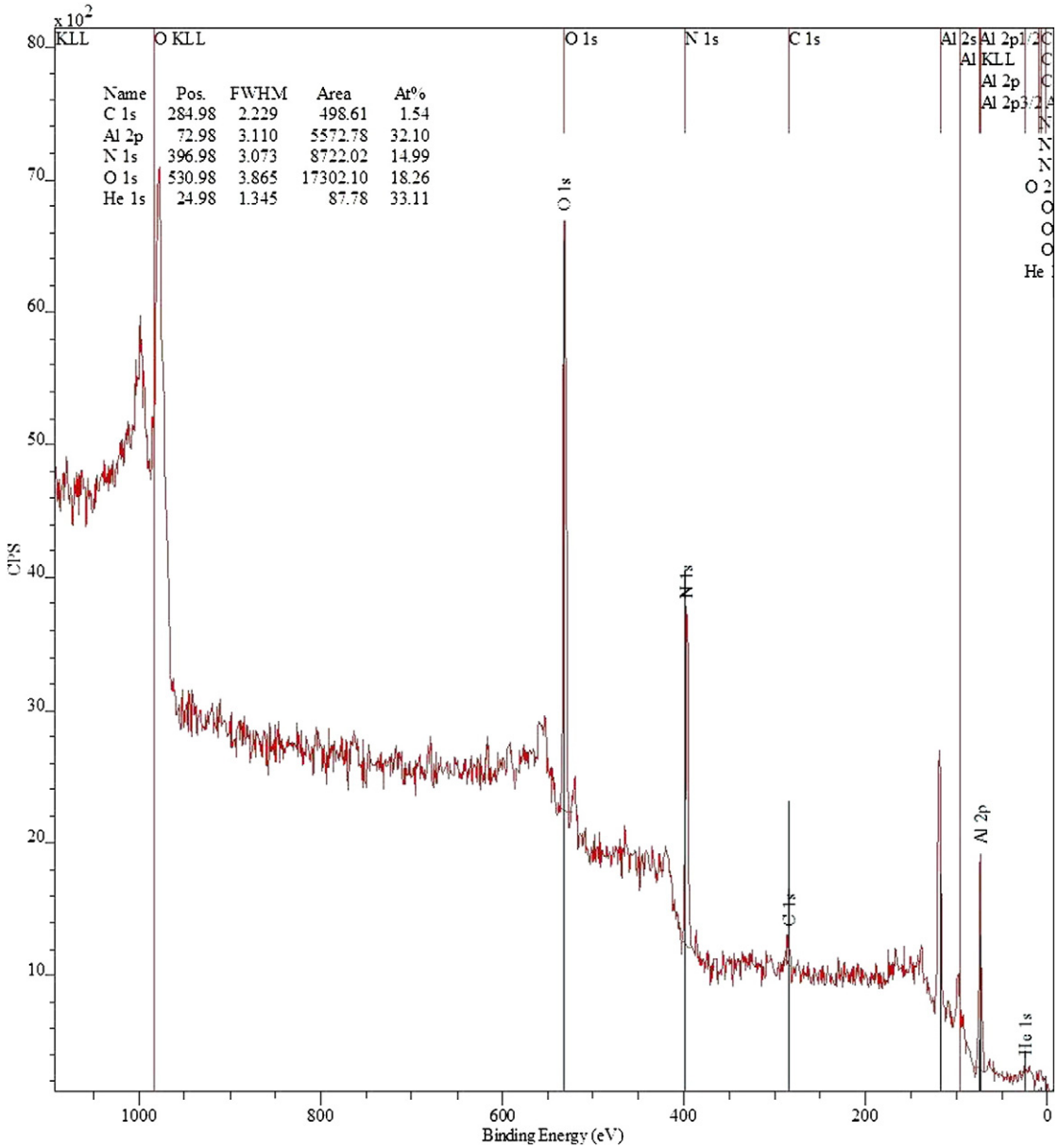

Fig. 4. XPS spectrum for alumina coating on stainless steel substrate via ECAP. Input microwave power setting for this sample was 1500 W. Spectrum pre-sputtered for 30 s to remove surface contaminants.

power, the gas flow rate and the type of processing gases introduced. In helium plasma, the APPT plasma could usually self-ignite to generate APP with a helium flow between 10 and 30 L/min, but an igniter could also be used. Pure argon, nitrogen or air APP can be also is obtained by first igniting the helium plasma, then mixing each of them into the helium and then slowly turning the helium off. This is critical from an economic viewpoint.

The aluminum target used is a 99.99% + pure aluminum obtained from the Kurt J. Lesker Company. It is in the form of cylinder pellets, with 1/8 inch (3.175 mm) diameter × 1/8 inch (3.175 mm) height. Aluminum pellets with high purity will be required since the deposition rate of aluminum oxide decreases as impurity within the target increases. Aluminum alloy (99% pure aluminum) samples (1000 series) were tested and the deposition rates were close to negligible.

A bottleneck was also created about 1/8 inch (3.175 mm) below the tip of the tungsten antenna. The diameter of the antenna is reduced from the normal 1/4 inch (6.35 mm) to around 0.1 inch (2.54 mm), and the height of this bottleneck is around 0.1 inch (2.54 mm) as well. The purpose of this bottleneck is to reduce the thermal conductivity and thus the heat transfer from the tip to the bottom of the antenna, as the APP plasma are generated at the tip, and it would be the hotter than the bottom end where no plasma is formed. From Fourier's law: $dQ/dt = -UA\Delta T$, where dQ/dt is the amount of heat transferred per unit time in W, U is the conductance in W/m^2 K, A is the cross-sectional area in meter squares and ΔT is the temperature difference between the two ends in Kelvin. By reducing the diameter of the antenna from 0.25 inch (6.35 mm) to 0.1 inch (2.54 mm), at the neck, the heat lost through the antenna is reduced by 84% ($1-(0.1/0.25)^2$). Indeed, the Al samples easily melts and evaporates with the necked antenna in place and does not if the neck is absent.

The substrates used are 304 stainless steel as they are readily available and could remain chemically inert while sustaining the high

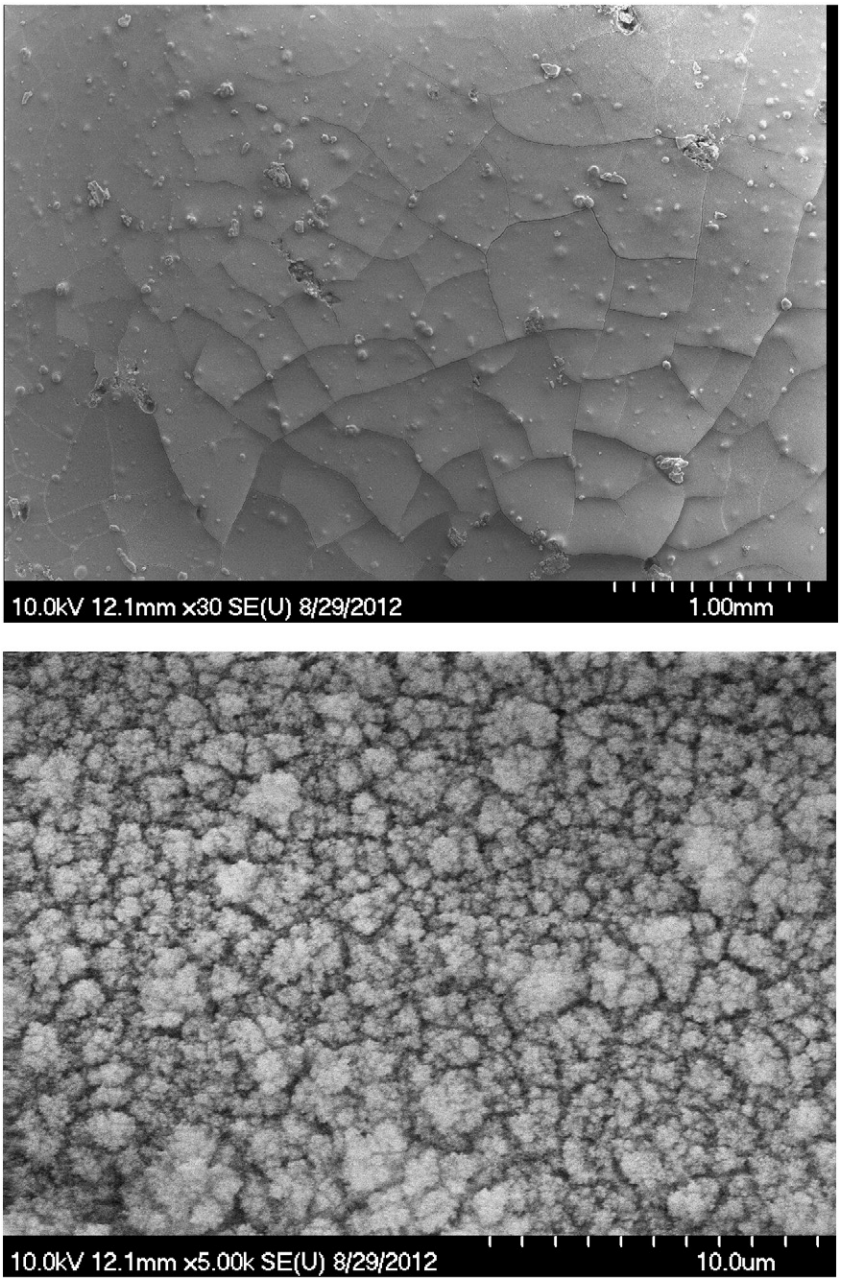

Fig. 5. SEM images for alumina coating on stainless steel substrate via ECAP. Top: low magnification (30×). Bottom: high magnification (5000×). Microwave power input was 800 W.

gas temperature of the APP. They are machined to 1-inch (25.4 mm) diameter discs and are mounted onto a homemade stainless steel substrate mount. The sample is then put on top of the APP for about 30 s to obtain alumina coating (Fig. 3). The size for the substrate is chosen to be 1-inch diameter so that it could have a large surface area for collecting aluminum vapors yet easily fit into various stage holders for tools used in thin film characterizations. In this study, XPS, SEM, FIB, XRD, TEM techniques were used to characterize the aluminum oxide film deposited with the APPT.

3. Results and discussions

3.1. X-ray photoelectron spectroscopy (XPS)

An XPS system (Physical Electronics PHI 5400) was used to determine the elemental composition on the film surface (Fig. 4). The sample measured was coated with 1500 W input microwave power, 15 L/min He and 3 L/min N_2 for 30 s. Both aluminum and oxygen peaks are observed in the spectrum and their atomic percentage (32.% for Al and 18.% for O in the spectrum). The small carbon peak was from organic contaminants in the air after the deposition, and its well-known binding energy of 285 eV was used for calibrating the spectrum for other elements. The nitrogen and oxygen peaks were from the outgassing from the film surface, as they are the processing gases in the deposition process. Outgassing occurs since the morphology of the film was porous, as shown in FIB image later. Aluminum nitride AlN could not form on the substrate surface in this sample since AlN will start decompose at temperature above 1370 °C and bulk oxidization will occur, turning it into aluminum oxide. The substrate surface temperature was found to be above 1400 °C, as shown in COMSOL simulations later. From the XPS spectrums it can be concluded that aluminum oxide is being deposited onto the stainless substrate with ECAP using the APPT.

3.2. Characterization of film morphology using scanning electron microscope (SEM)

Under SEM images (Hitachi S-4700 High Resolution SEM), the deposited alumina film showed microscopic crack across the film surface, and some local delamination seems to occur as well (Fig. 5). This is probably due to the dramatic change of substrate temperature at the end of the alumina film deposition. The APPT plasma with 80% helium and 20% nitrogen will produce a gas temperature around 1000–1500 °C with 800 W input power, and it will be rapidly cooled to room temperature after deposition. This thermal shock and the difference in thermal expansion coefficient between 304 stainless steel and alumina would thus cause the film to crack and delaminate from the surface. At higher magnification, the film morphology looks porous and small spheres seems to be forming clusters on the film surface as well.

3.3. Focused Ion Beam (FIB)

From the FIB images (FEI Dual Beam 235 FIB), the morphology of the alumina sample deposited with 800 W input microwave power was found to be completely porous, all the way through from the surface of the film to the film-substrate interface (Fig. 6). Film thickness was determined to be around 1 μm for a 30-s deposition, and thus the deposition rates for the samples under these conditions are around 2 μm/min.

When the sample deposited with 1500 W input microwave power was put under the FIB imaging system, no image could be obtained due to severe surface charging. Since alumina is a ceramic material and an insulator, electrons or ions from the FIB source will slowly charge up on the surface and image contrast would be lost. This surface charging phenomena was not observed in the porous alumina film deposited with 800 W microwave power, however. This raised

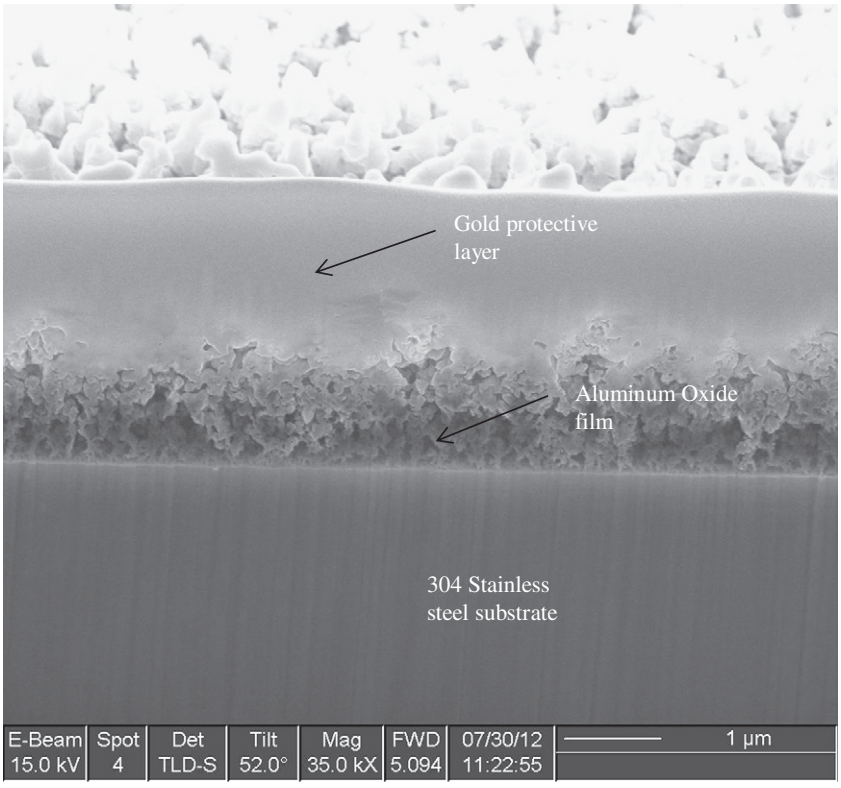

Fig. 6. A close up FIB image showing the porous structure of the alumina coating at 800 W power on stainless steel substrate.

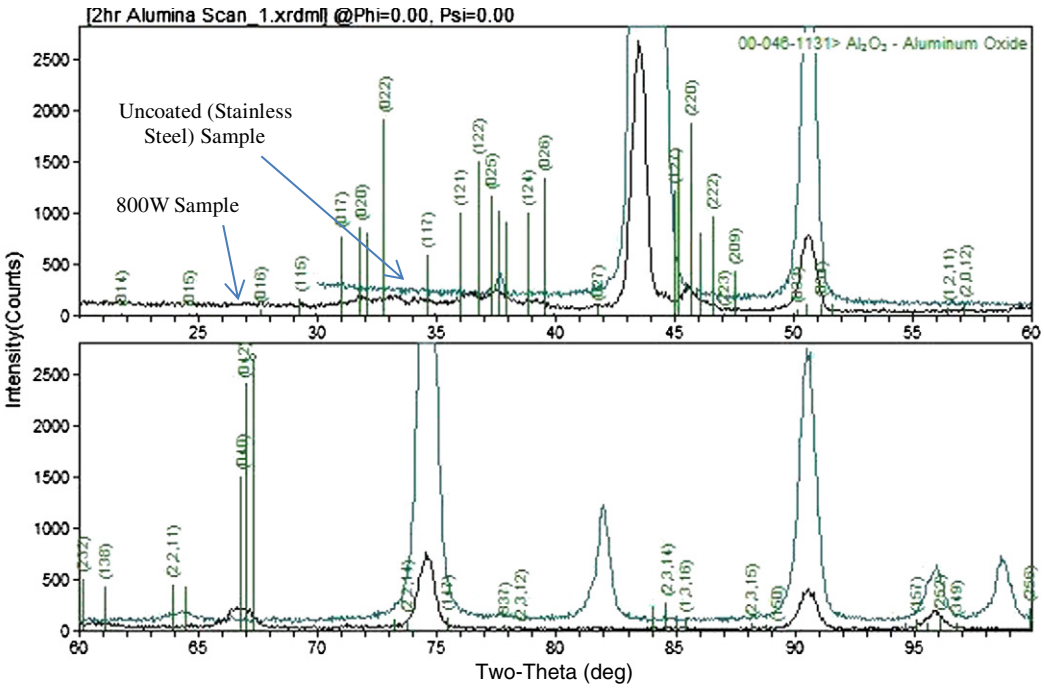

Fig. 7. XRD spectrum for the 800 W alumina sample. The closest match for this spectrum is alumina in δ phase.

suspicion that the morphology of the film made with 1500 W microwave power may be of a different phase or a structure that is denser than the one found in 800 W, which would have more surface coverage and caused surface charging on the FIB system. Therefore, in order to resolve this alumina phase problem, an X-ray diffraction run was performed to find out whether the alumina coating obtained in ECAP are amorphous or crystalline, and whether the phase of the alumina would be different at different microwave power levels.

3.4. X-ray diffraction measurements (XRD)

XRD spectrums were taken using Philips X'pert MRD system. The XRD spectrum for the 800-W samples matches the spectrum of the δ phase alumina the closest, and the spectrum of the β phase turns out to be the closest match for the 1500-W sample (Figs. 7 and 8). However, none of the alumina phases in the XRD library matches the spectrum perfectly. The spectrum of AlN and AlON were also compared to check for the possibility of nitride formation, and they did not match the sample spectrum either. Thus, the only remaining logical explanation for these imperfect match sample XRD spectrums could be that these deposited alumina films actually consisted of a mix of alumina phases, and the most predominant phase in the film will show up as the closest match to the sample. Transmission electron microscope is thus used to determine whether the above assumption was true and there indeed more than one phase coexisted on the alumina film samples.

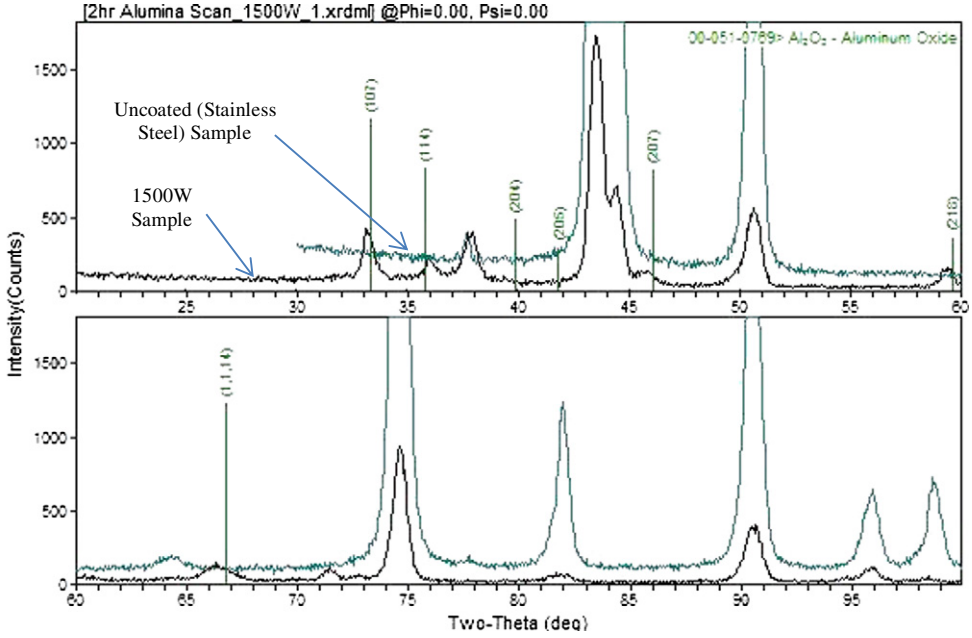

Fig. 8. XRD spectrum for the 1500 W alumina sample. The closest match for this spectrum is alumina in β phase.

Table 1
The *d*-spacing for various alumina phases.

Beta	(hkl)	Gamma	(hkl)	Theta	(hkl)	Delta	(hkl)	Chi	(hkl)	Alpha	(hkl)	Kappa	(hkl)
2.8	1 1 0	2.8	1 1 0	5.7	2 0 0	2.8115	0 2 0	1.98	4 0 0	2.3801	1 1 0	4.1826	1 1 0
1.845	2 1 0	1.977	4 0 0	1.9094	6 0 0	1.986	2 2 0			1.3742	3 0 0	3.1553	1 2 0
		1.395	4 4 0	1.7998	5 1 0	1.771	1 3 0			1.1901	2 2 0	2.4192	2 0 0
		0.989	8 0 0	1.4526	0 2 0	1.3996	0 4 0			0.8996	4 1 0	2.4055	1 3 0
		0.884	8 4 0	1.4264	7 1 0	1.0969	1 5 0					2.3233	2 1 0
						1.0398	2 5 0					2.0795	0 4 0
												1.9102	1 4 0
												1.8232	2 3 0
												1.3943	3 3 0
												1.3863	0 6 0
												1.0512	3 6 0
												0.8365	5 5 0

3.5. Transmission electron microscope (TEM)

A JEOL 2100 Cryo TEM system was used to obtain TEM images for this study. To determine the phase from these TEM images, first the *d*-spacing of all different types of aluminum oxide is obtained from the XRD library. Since the image from the TEM is a two dimensional image, only crystal plane that is parallel to the *z*-axis are considered (i.e. $l = 0$). The atomic spacing that is measured from the image is

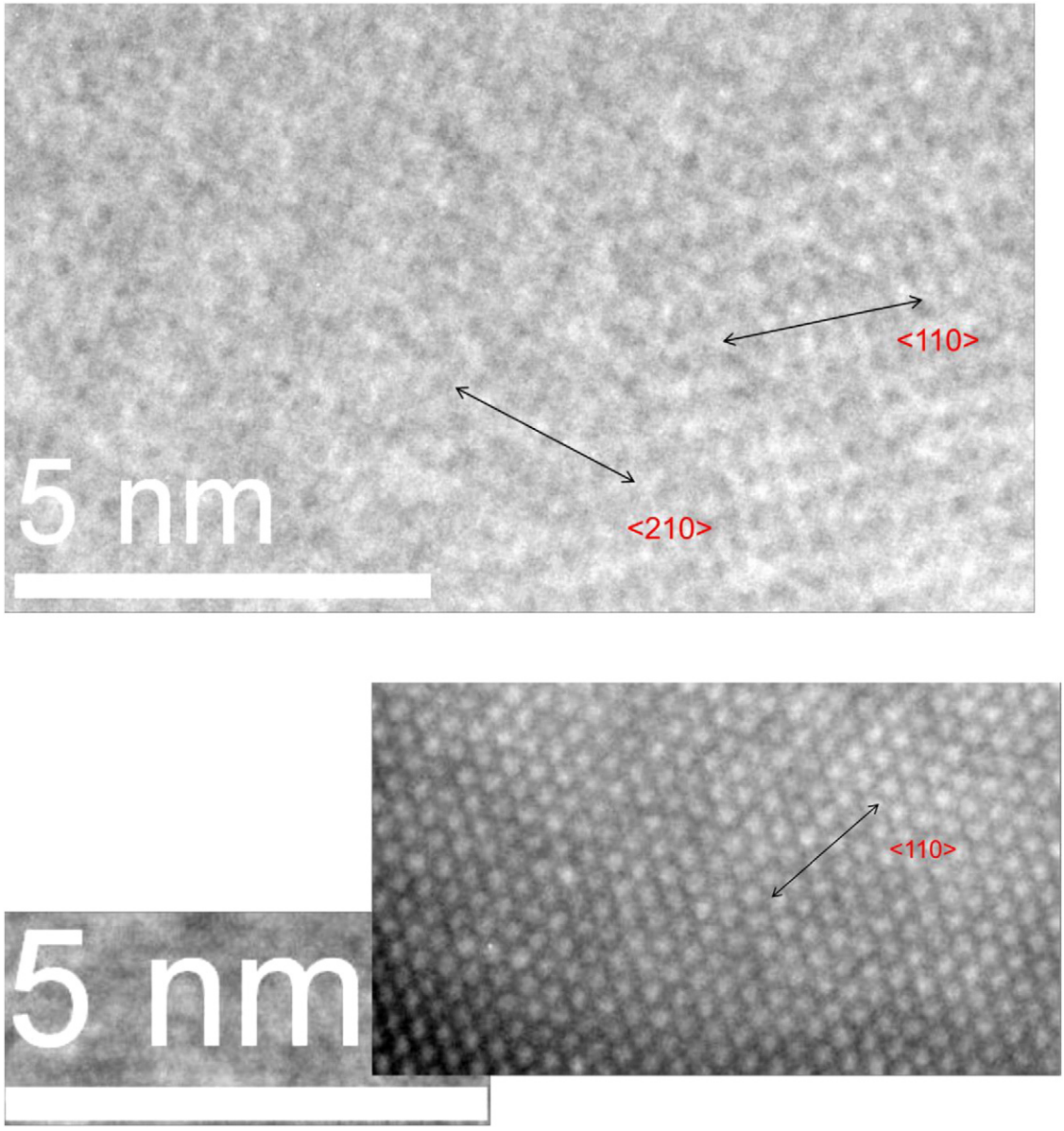

Fig. 9. TEM images for determining the phase of ECAP deposited alumina. Top: 800 W and bottom: 1500-W samples, with crystal plane direction indicated on the image.

related to the *d*-spacing used in crystallography through a simple equation: $a = d\sqrt{\circ\left(h^2 + h^2 + l^2\right)}$, where a is the atomic spacing, d is the *d*-spacing and *h*, *k*, *l* and the Miller indexes. Fortunately, all phases except beta and gamma have a different atomic spacing, so comparing one to two spacing in the image is generally sufficient to determine the phase of alumina in the image. The *d*-spacing for various alumina phase and the Miller indexes are listed in Table 1 [14–20].

For the 800-W sample, the atom spacing was measured to be around 3.960 Å between the adjacent atoms, this matches the (110) plane for the beta and gamma phase. The next closet atom was then measured to differentiate between beta and gamma, and it was measured to be 4.13 Å and matches the (210) plane for the beta phase; thus, the crystal in the sample was beta alumina. Similarly, for the 1500-W sample, the distance between adjacent atoms was measured to be 3.365 Å, and that matches with the (110) plane of the alpha alumina; thus, the crystal in that sample was in alpha phase (Fig. 9). In both cases, the crystal is in a difference phase than the XRD predicted. Thus, the TEM analysis confirmed there were more than one crystal phase present in both alumina thin film samples made by ECAP.

3.6. COMSOL computer simulation

The standard turbulent flow kappa-epsilon model was thus used to determine the gas flow inside the APPT, since the Reynolds number was found to be around 3000 for the flow rate used in the experiment. It first calculates the turbulent kinetic energy κ and dissipation energy ε in the fluid transport equation. Then the turbulent velocity μ can be calculated, since $\mu = \rho C\kappa^2/\varepsilon$, where ρ is the fluid density and C is an empirical determined constant around 0.09. The input flow was set to be 1.2×10^{-4} kg/s for helium and 6.36×10^{-5} kg/s for nitrogen, corresponding to 15 and 3 L/min air equivalent flows, respectively. The COMSOL simulation estimated the gas velocity in the APPJ quartz tube to be around 0.7 m/s throughout most part of the tube, and there is an increase in velocity around the tip of the antenna up to around 0.9 m/s due to the change of shape at the tip of the antenna (Fig. 10). Predicted flow velocities at the antenna tip for various input flow rate are shown in Fig. 11.

By coupling the previous turbulent flow model and the RF microwave heating module, which solves for the electric field distribution

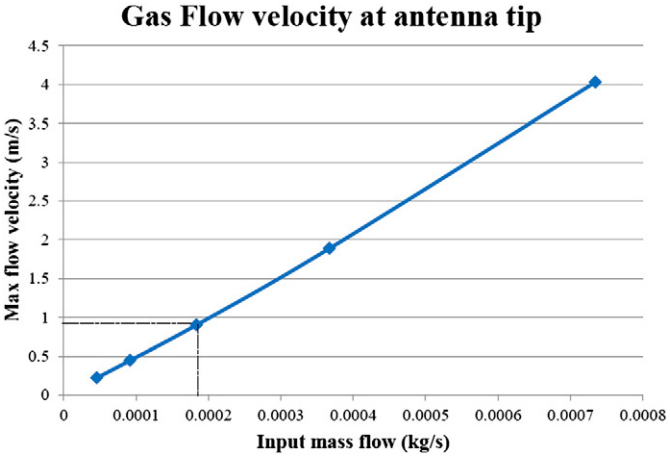

Fig. 11. Predicted gas flow velocity at the antenna tip by COMSOL simulation. Condition of flow in Fig. 10 is shown by the dotted lines.

and dielectric heating inside the APPJ, the plasma gas temperature was also simulated for the 800-W and 1500-W microwave input power case. To account for the reflected power, a USB microwave power sensor (Mini-Circuits, Model PWR-SEN-6G+, USA) was used to monitor the reflected power in the waveguide. In both cases, the reflected power was measured to be around 10% of the input power, and thus the values of the net input power used for the simulation were 720 and 1350 W for the 800-W and 1500-W case, respectively. The temperature of the 800-W case was simulated to be around 1700 °C and 1000 °C at the top of the target and the location of the substrate (solid black line near the top of Fig. 12), respectively. For the 1500-W case, the temperature was simulated to be around 2900 °C and 1400 °C, respectively. Predicted temperature at the substrate center and maximum plasma temperatures for various microwave power input are shown in Fig. 13.

The temperatures obtained from the COMSOL simulation seems to be physical since in both cases they are close or above the boiling point of aluminum and allow evaporation to occur. The temperature at the substrates also stays below the melting point of the 304 stainless steel. This agrees with the experimental observations since no substrate melting was observed in the ECAP experiment.

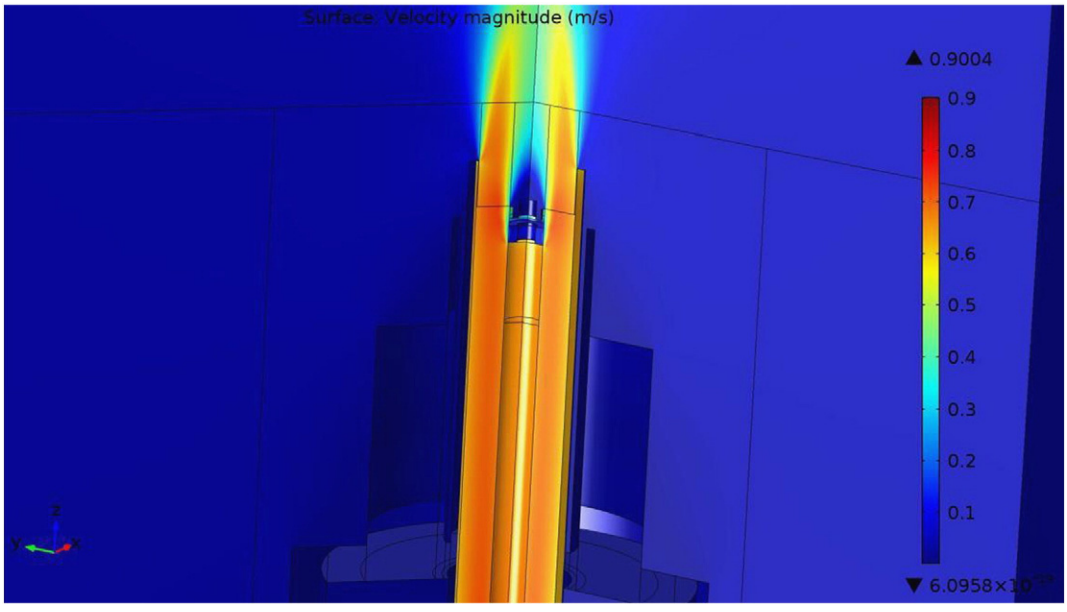

Fig. 10. COMSOL simulation image for gas flow profile inside the APPJ. The highest rate of flow was located at the area outside the tip of the antenna at around 0.9 m/s.

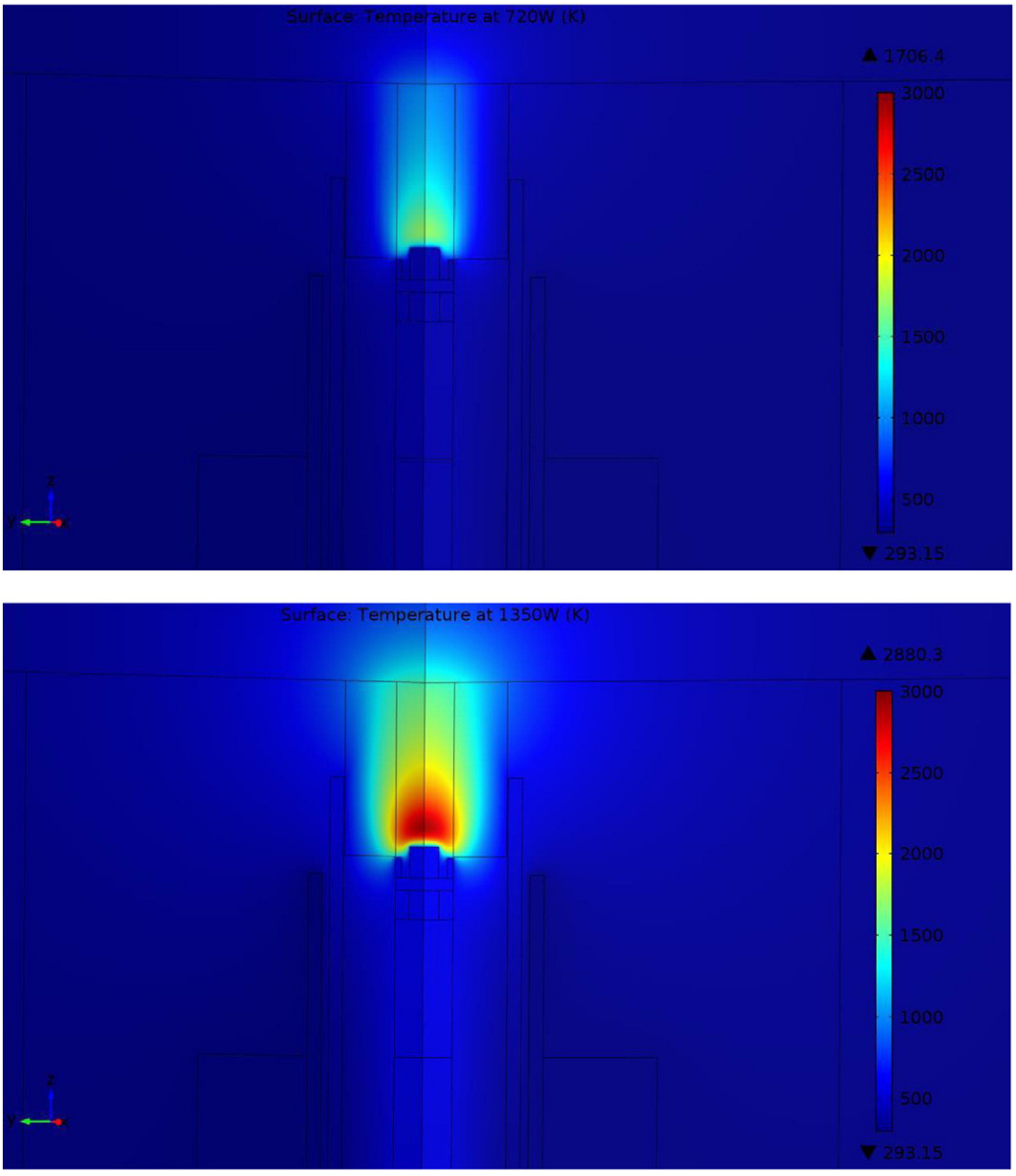

Fig. 12. COMSOL simulation image for plasma temperature profile of APPJ at (Top) 800 W and (Bottom) 1500 W input power.

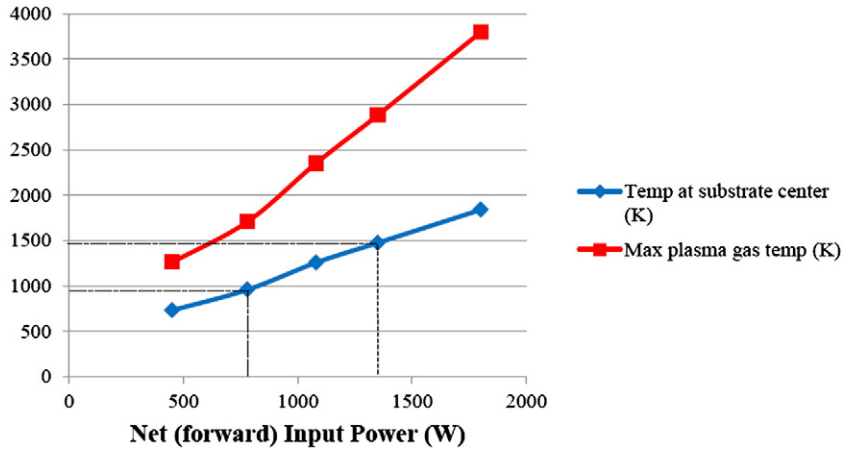

Fig. 13. Predicted temperature at the substrate center and maximum plasma temperature by COMSOL simulation. Temperature profile in Fig. 12 are shown by the dotted lines.

The APPT temperature simulation results could also explain the different phases observed in the coatings made with different microwave power settings. The temperatures at the substrate were 1000 °C for the 800-W sample and 1400 °C for the 1500 W one. With reference to the transition sequence as described in Fig. 1, δ phase could be formed in temperature between 700 °C to 1050 °C and the α phase would be observed in temperature above 1100 °C. Both the δ phase and the α phase were observed in previous characterization results in the 800-W sample and 1500-W sample, respectively, and the simulated temperatures were in good agreement with the alumina phases obtained in the experiment.

4. Conclusion

Aluminum targets have been evaporated using microwave APPT in the ECAP experiment. It was demonstrated that aluminum oxide could be successfully coated onto 304 stainless steel substrates using ECAP with helium and nitrogen gas mix and APP microwave plasma. Only a high-purity aluminum target could produce aluminum oxide coating at an observable rate. The techniques of XPS, SEM, FIB, XRD and TEM were used to characterize the alumina film formed using this deposition method. The film was confirmed to be aluminum oxide from the elemental composition. The film morphology was found to be porous under low power deposition but denser under high power deposition conditions. The deposition rate of the process was found to be around 2 μm/min. Nitrogen and helium was also found on the film surface as they were outgassing from the porous film during XPS measurements. The δ phase and the β phase alumina was found in the 800-W sample, and the β phase and the α phase alumina was found in the 1500-W sample. The phase of the deposited alumina film was determined to vary according to changes in input microwave power, and more than one phase of alumina could simultaneously form in the alumina film, in the form of nanocrystal, and could be seen under TEM images. Different phases of alumina nanocrystal could be identified by measuring the *d*-spacing on the TEM images and comparing them to the known data spacing values of various phases.

The plasma gas and temperature profile of the microwave APPJ was simulated using finite element analysis simulation software COMSOL. The Reynolds number was calculated to be around 3000 and the flow inside the APPT was in turbulent regime. The standard turbulent flow kappa epsilon model was used to model this turbulent flow inside the APPT. The flow profile was found to peak around the antenna tip. By coupling the turbulent flow model and the RF microwave heating model, the dielectric heating inside the APPT and thus the temperature profile was simulated. The temperature profile was found to be close to the boiling point of the alumina at the target surface and below melting point of the 304 stainless steel at the substrate surface. The temperature profile also correctly predicted the different phases obtained for samples prepared with different input microwave power.

References

[1] Zihao Ouyang, et al., J. Phys. D: Appl. Phys. 44 (2011) 265202.
[2] Jon Martin Anderson, Controlling the Formation and Stability of Alumina Phases, 2005.
[3] I. Levin, D. Brandon, J. Am. Ceram. Soc. 81 (1998) 1995.
[4] C. Misra, Industrial Alumina Chemicals, ACS Monograph, 184, American Chemical Society, Washington, D.C., U.S.A., 1986
[5] I. Levin, D. Brandon, J. Am. Ceram. Soc. 81 (1995) (1998).
[6] W.H. Gitzen, Alumina as a ceramic material, The American Ceramic Society, Westerville, 1970. 17.
[7] X. Multone, High Vacuum Chemical Vapor Deposition of Alumina Thin Films, 2009.
[8] Z. Ouyang, Deposition of yttria-stabilized zirconia thermal barrier coatings by laser-assisted plasma coating at atmospheric pressure, 2011.
[9] K. Iida, T. Tsujide, Jpn. J. Appl. Phys. 11 (6) (1972) 840.
[10] W.C. Oliver, G.M. Pharr, J. Mater. Res. 7 (1992) 1564.
[11] Y. Sato, S. Akimoto, J. Appl. Phys. 50 (1979) 5285.
[12] R.H. French, J. Am. Ceram. Soc. 73 (1990) 477.
[13] Angus Rockett, The materials science of semiconductors, Springer, 2010.
[14] A. Meisel, Private communication, Karl-Marx University, Leipzig, Germany, 1956.
[15] Rooksby, X-ray Identification and Crystal Structures of Clay, 1951. 264.
[16] Yamaguchi, et al., Bull. Chem. Soc. Jpn. 43 (1970) 2487.
[17] Y. Repelin, E. Husson, Mater. Res. Bull. 25 (1990) 611.
[18] Stumpf, et al., Ind. Eng. Chem. 43 (1950) 1398.
[19] J. Lewis, D. Schwarzenbach, H.D. Flack, Acta Crystallogr. A Cryst. Phys. Diffract. Theor. Gen. Crystallogr. 38 (1982) 733.
[20] M. Halvarsson, V. Langer, S. Vuorinen, Powder Diffract. 14 (1999) 61.
[21] F.M. D'Heurle, Metall. Trans. 1March (1970) 725.
[22] W.D. Sproul, M.E. Graham, et al., J. Vac. Sci. Technol. A 13 (3) (1995) 1188.